Journal of ELECTRICAL ENGINEERING, VOL 55. NO 10/S, 2004, 66-69

MEASUREMENT OF LOCAL ELECTRIC AND MAGNETIC QUANTITIES INSIDE ELECTRICAL INDUCTION MOTORS

Oriano Bottauscio[*] — Mario Chiampi[**] — Lorenzo Donadio[*] — Mauro Zucca[*]

The development of more and more accurate numerical models for the analysis of the electromagnetic phenomena occurring inside electrical induction motors calls for the availability of experimental validations to be obtained in laboratory tests. The requirement of an experimental validation cannot be limited to integral quantities (supply currents, input power, etc.), but also to local physical quantities inside the machine, such as magnetic fluxes in stator and rotor core and currents flowing in the rotor cage. The comparison of computed and measured results allows a deep insight on the capability of the mathematical model to accurately reproduce the phenomena, and consequently of predicting the device performances and in particular the power losses under different operating and supply conditions.

Keywords: induction motors, current transducers, rotational fluxes.

1 INTRODUCTION

Evaluation of losses in induction motors is a matter of industrial (improve the motor efficiency) and academic (advanced modelling of electromagnetic phenomena) interest [1, 2, 3]. The loss estimation in induction motors is conventionally performed by the well known short-circuit test, to evaluate the so called "copper losses" and no-load test, to evaluate the so called "iron losses". The outcomes of these two tests can be conveniently obtained by an advanced numerical tool or measured using an experimental set-up. In particular, concerning the no-load test, numerical tools have the advantage of allowing an easy loss separation between stator and rotor losses and a deep analysis of the motor performances. This work is devoted to the analysis of the motor behavior under no-load test conditions at synchronous velocity. This investigation is made arduous by the presence of:

- strong magnetic saturation in the core;
- rotational fluxes that cause additional contribution to magnetic losses;
- high harmonic flux pulsation that are responsible for induced currents in the rotor cage;
- interaction between electromagnetic field and electric circuit;
- skin effect in the laminated cores.

A recent approach for modelling no-load test, presented by the authors in [4], is based on the following characteristics:

1. voltage driven electromagnetic field problem handled by Finite Element Method;
2. time evolution analysed through a step by step process;
3. rotor displacement accounted for by means of the "Sliding Mesh Technique";
4. magnetic behavior of the material included by the first magnetisation curve and handled by the Fixed Point Technique;
5. skin effect in laminations given by the solution of 1D electromagnetic field problems in the sheet thickness;
6. excess and static losses deduced by the loss theory.

The presence of several and complex phenomena makes the model validation particularly important. To this end, the evaluation of integral quantities is not sufficient and the execution of magnetic measurement inside stator and rotor cores and electric measurement on the rotor cage is required. All these measurements have been performed, under controlled conditions, on a specific set-up achieved at IEN [5].

2 EXPERIMENTAL SET-UP

In order to experimentally investigate the magnetic behavior of induction motors, a specific device has been realized. The experimental device is composed of a four-poles three-phase stator (36 slots) of a 7.5 kW motor, where two laminations have been equipped with pick-up coils, for the measurement of local flux density waveforms (see Fig.1). Particular attention has been devoted to the rotational fluxes, which are generated in the yoke at the tooth root.

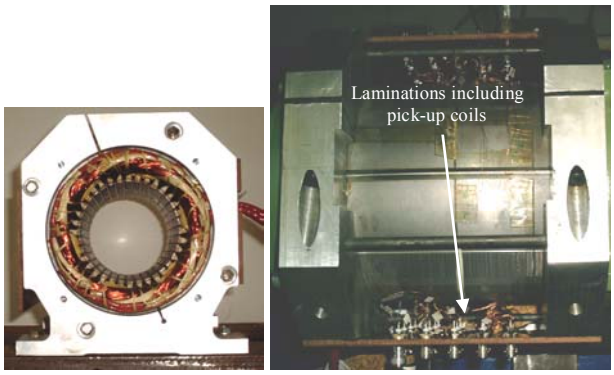

Fig. 1. Fitted stator of the induction motor

[*] Istituto Elettrotecnico Nazionale G. Ferraris strada delle Cacce 91, I-10135 Torino (Italy) - [**] Dipartimento di Ingegneria Elettrica Industriale, Politecnico di Torino, corso Duca degli Abruzzi 24, I-10129 Torino, Italy, zucca@ien.it

ISSN 1335-3632

The device can mount two kinds of rotors with 48 slots: the first one is a cage-less rotor with pick-up coils disposed on a lamination to measure the magnetic flux pulsation in the rotor teeth without the armature reaction (see Fig. 2c).; the second one is equipped with a cage, where suitable current sensors have been housed to measure the induced current waveforms (see Fig. 2a and b). In both cases the signals have been kept outside the rotor thanks to a commercial slip ring capsule (10 circuits) connecting the hollow shaft with the stationary structure.

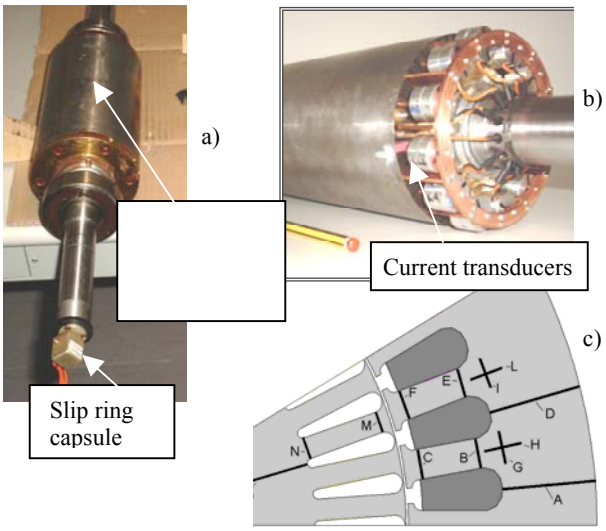

Fig. 2. a) rotor without cage, b) rotor fitted with current transducers, c) stator and rotor pick-up coils location

A synchronous motor guarantees the rotation of the rotor with the main field. An electronic device, generating a three-phase voltage system with different waveforms (sinusoidal, six-step, twelve-step, etc.), supplies in parallel the synchronous and the induction motors in order to achieve a no-load test at synchronous speed.

2.1 Current transducer choice

The spatial distribution of magnetic flux density in the air gap computed with reference to the stator frame is evidenced in Fig. 3. The first harmonic of the spatial magnetic field distribution is stationary with respect to the rotor, but the superimposed ripple, generated by the presence of the stator slots, produces a magnetic flux ripple in the rotor teeth if the rotor is without cage, and a current in the bars in the rotor with cage. An example of calculation of these currents shows how the intensity of the phenomenon in a given rotor tooth depends on its position with respect to the main magnetic field that is synchronous with the rotor, as evidenced by Fig. 4. This implies that the e.m.f. induced in the bars are dependent on the position of the bar itself; so the corresponding bar currents vary from a minimum ("low bars") to a maximum ("high bars") as it is shown in Fig. 5.

The bar current measurement is made complex by the limited space available for the housing of the transducers, by the high current levels (~100 A) and by the strong harmonic contents depending on the stator tooth number.

Different solutions for the current transducer have been considered. The use of resistive shunts has been avoided because they can alter the current sharing between the bars. Also amperometric transformers are no suitable for the purpose because of the restricted distance between rotor and motor cap, that limits the diameter and thickness of the transducer core giving rise to unavoidable saturation. Rogowski coils and Hall-effect probes can be affected by the presence of stray field generated by the electronic supply and by the bars surrounding the transducer. Eventually, the adopted solution consists of a coil winded on a soft ferrite annulus placed around the bar under analysis (see Fig. 6).

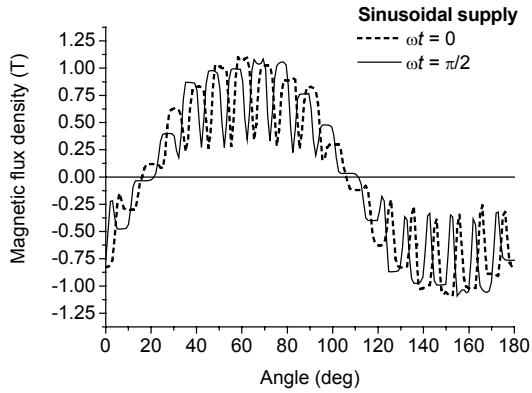

Fig. 3. – Flux density in the air gap computed with reference to the stator frame

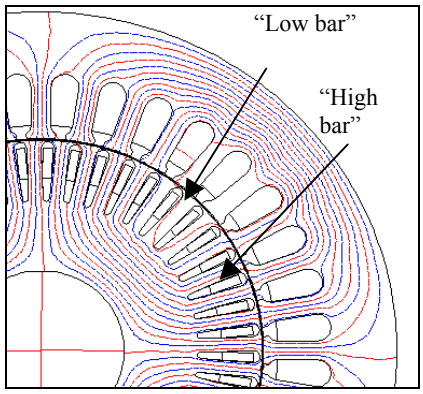

Fig. 4. Instantaneous magnetic flux distribution

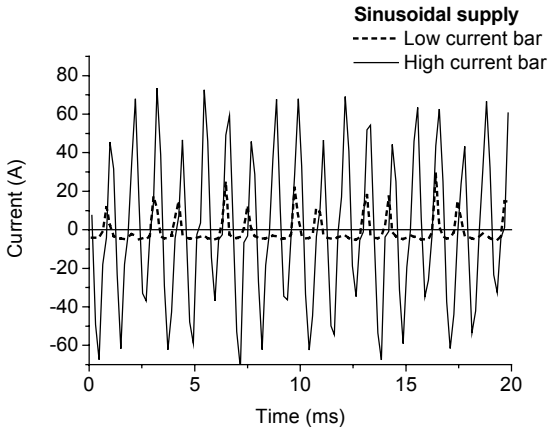

Fig. 5. Example of current waveforms in the rotor bars

The integration of the emf measured at the open terminals of the coils provides a waveform related to the current under measurement.

2.2 Current transducer design

In the adopted solution the core dimensions have been determined by the constraints introduced by the cage, which impose a maximum diameter of 19 mm. For a linear response of the transducer, a calibrated air-gap has been introduced in the ferrite core. The influence of the air-gap dimension on the transducer response has been evaluated by finite element electromagnetic field analysis.

The deformation of a sinusoidal current waveform, caused by core saturation, has been estimated by the Total Harmonic Distortion ($THD_{o/oo}$) index, defined as:

$$THD_{0/00} = 1000 \cdot \sqrt{\sum I_i^2 (r.m.s)} \Big/ \sqrt{I_1^2 (r.m.s)} \qquad (1)$$

where i is the harmonic order.

The transducer behavior has been computed for different values of the air-gap from 0.1 to 1.4 mm, evaluating the limit value of current for the linear response. Also the system sensitivity has been computed for each case. At the end a 0.6 mm air gap has been chosen, which provides a linear response up to ~120 A. The transducer has a constant sensitivity equal to 25 mV/A practically without phase error over the frequency range up to 5 kHz.

2.3 Current transducer shielding and calibration

Two disturbances have been analyzed by the FEM model:

1. the external disturbances and noise due to electric power sources;
2. the proximity effect due to the bars contiguous to the transducer.

The external disturbances due to stray fields have been simulated by introducing a 5 mT uniform field, whose frequency ranges from 1.8 kHz (36th harmonic) up to 10 kHz. The proximity effect has been modeled by imposing in the two surrounding bars the same current (100 A peak, 900 Hz) with the phase-shift due to their angular position.

The external noise effect can be mitigated inserting the transducer in a cylindrical ferromagnetic or pure conductive shield (see Fig. 6). In our case an aluminum shield has been chosen because the limited thickness imposed by geometrical constraints can cause saturation in ferromagnetic materials. The same shielding solution also reduces the proximity effect.

Twelve current transducers have been assembled, calibrated and finally mounted on the rotor. Half rotor slots, that is 24 slots, have been fitted by bars, twelve of them equipped with transducers (see Fig. 2b). Calibration has been performed inserting, in a specific position inside the transducer, a rectangular bar with the same section as the actual rotor. The transducer has been finally mounted on the rotor in the same relative position with respect to the bar as in the calibration phase.

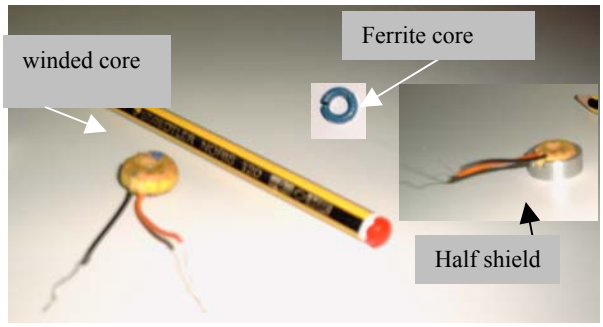

Fig. 6. Current transducer details

3 MEASUREMENT RESULTS AND MODEL PREDICTION COMPARISON

Computed and measured local magnetic and electric quantities have been compared in order to achieve a deep insight on the capability of the mathematical model to accurately predict the device performances. First of all the fluxes in stator and rotor yoke have been measured and computed reaching a quite perfect agreement between them. Then the analysis has been focused on the rotational fluxes at the stator tooth root measured under different supply waveforms. Fig. 7 presents the results in the case of a six-step and twelve step supply, showing a more than satisfactory agreement between measurements and computations. Also the magnetic flux pulsation inside the rotor teeth without the cage has been computed and measured under sinusoidal supply. Since the pulsation depends on the relative position between tooth and rotating field, the computed waveforms corresponding to the two limit conditions ("high" and "low" teeth) are presented in Fig. 8.

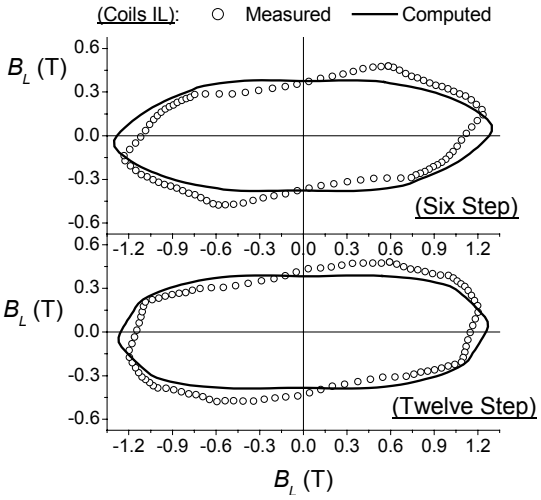

Fig. 7. Flux density loci at the tooth root

The analysis on the cage currents, reported in Figs. 9 and 10 for sinusoidal and six step supply respectively, allows to do the following considerations:

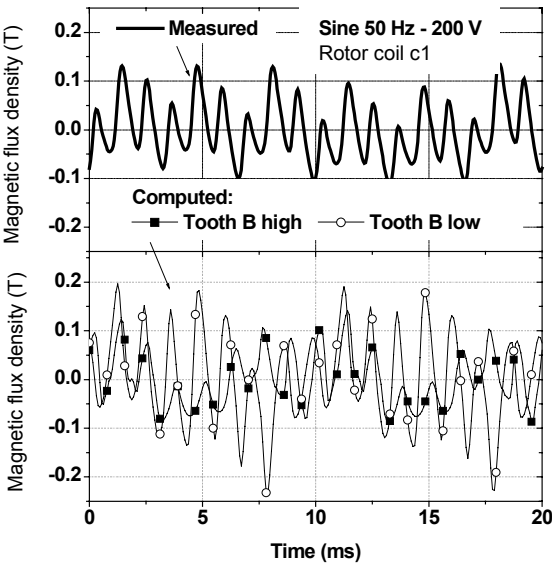

Fig. 8. Measured and computed flux pulsations inside the rotor teeth

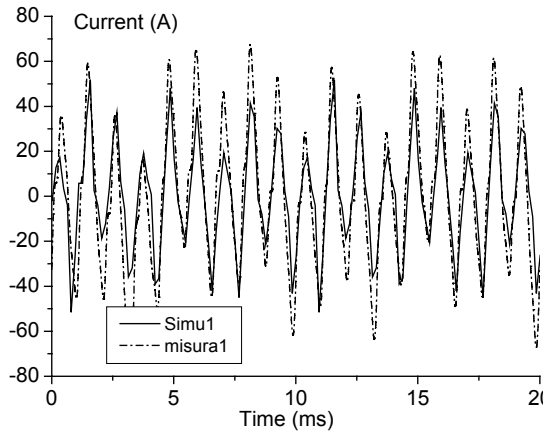

Fig. 9. Computed and measured current waveforms in the "high bar" under 50 Hz sinusoidal supply

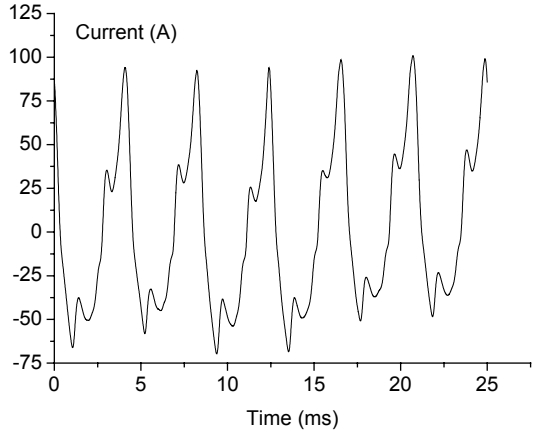

Fig. 10. Measured current waveform in the "high bar under 40 Hz six-step supply

- a good agreement between measurements and computations is found, showing the capability of the numerical model to reproduce the induced phenomena in the rotor cage;
- the harmonic spectrum of the currents evidences the presence of significant 6^{th} and 18^{th} harmonic components related to the number of stator teeth;
- despite the analysis has been performed at synchronous speed, the current amplitude reaches ~ 70 A. This value could further increase for an actual motor having a cage with lower resistance;
- under non sinusoidal supply waveforms the bar currents even more increase, as shown in Fig. 10 for a six-step supply; here the current amplitude reaches the similar values as under sinusoidal supply, even if the voltage and frequency have lower values.
- cage currents are responsible for additional losses in the rotor cage under any operating condition and their predictions can provide a more detailed description of the energetic behavior of the motor.

4 CONCLUSIONS

The laboratory set-up here presented allows a detailed experimental analysis of electric and magnetic quantities within an induction motor. The measured results have been compared with the predictions given by an advanced FEM code, achieving a more than satisfactory agreement.

The comparison between computed and measured results have put in evidence the capability of the model to reproduce the local magnetic and electric phenomena. This is a primary aspect in the development of tools able to predict, in an accurate way, the power losses under different operating and supply conditions and, consequently, of improving the efficiency of the induction motor

REFERENCES

[1] GYSELINCK J.J.C., VANDEVELDE L., MAKAVEEV D., MELKEBEEK J.A.A.: Calculation of no load losses in an induction motor using an inverse vector Preisach Model and an eddy current loss model, IEEE Transaction on Magnetics., 36, No 4, (2000), 856 - 860.

[2] ENOKIZONO M., OKAMATO K.: Designing a low-loss induction motor considerino the vector magnetic properties, IEEE Transaction on Magnetics., 38, No 2, (2002), 877 - 880.

[3] SAITZ J.: Computation of the core loss in an induction motor using the vector Preisach hysteresis model incorporated in finite element analysis, IEEE Transaction on. Magnetics, 36, No. 4, (2000), 769-773.

[4] BOTTAUSCIO O., CHIAMPI M., MANZIN A., ZUCCA M: Additional Losses in Induction Machines under Synchronous No-Load Conditions, to appear on IEEE Transaction on Magnetics

[5] BOTTAUSCIO O., CHIAMPI M., ZUCCA M.: Experimental and numerical investigations on rotational fluxes in stator cores of three-phase motors, IEEE Transaction on Magnetics 38 No. 5, (2002), 3294-3296.

Received 28 June 2004